JOURNAL OF MATERIALS SCIENCE 29 (1994) 1991–1998

Structural properties of precipitates formed by hydrolysis of Fe^{3+} ions in $Fe_2(SO_4)_3$ solutions

S. MUSIĆ, Z. OREHOVEC, S. POPOVIĆ*
*Ruđer Bošković Institute, P.O. Box 1016, 41001 Zagreb, * and also Department of Physics, Faculty of Science, P.O. Box 162, 41001 Zagreb, Croatia*

I. CZAKÓ-NAGY
Department of Nuclear Chemistry, Eötvös-Loránd University, P.O. Box 32, 1518 Budapest, Hungary

The structural properties of the solid phase, formed by the hydrolysis of Fe^{3+} ions in $Fe_2(SO_4)_3$ solutions at 90 or 120 °C, were investigated using X-ray diffraction, ^{57}Fe Mössbauer spectroscopy, Fourier transform–infrared spectroscopy (FT–IR) and transmission electron microscopy. The concentration regions of $Fe_2(SO_4)_3$ were determined for the precipitation of goethite, α-FeOOH, or hydronium jarosite, $H_3OFe_3(OH)_6(SO_4)_2$, as a single phase. Superparamagnetic behaviour of α-FeOOH particles was observed. Hydrolysis of Fe^{3+} ions in 0.1 M $Fe_2(SO_4)_3$ solutions at 120 °C produced $H_3OFe_3(OH)_6(SO_4)_2$ and basic sulphate, $Fe_4(OH)_{10}SO_4$. The interpretation of ^{57}Fe Mössbauer and FT–IR spectra is given.

1. Introduction

Precipitation of iron(III) oxyhydroxides and oxides from Fe(III)-salt solutions has been studied by many authors. It was observed that the phase composition of precipitate, morphology and particle size depended on different factors, such as the concentration of Fe(III)-salt, pH, temperature, precipitation time, etc. For the same concentration of Fe^{3+} ions and the same conditions of slow hydrolysis, the nature of the corresponding anion (Cl^-, F^-, ClO_4^-, NO_3^-, SO_4^{2-}) may change the phase composition of hydrolytical products, as well as the shape of the particles.

Investigation of the influence of sulphate anions on the precipitation of iron(III) oxyhydroxides and oxides is important from the practical point of view (pigments, catalysts, atmospheric corrosion, etc.). For instance, the phase composition of the rust, generated during the atmospheric corrosion of steel, and the corresponding phase transformations, were dependent on the presence of SO_2/SO_3 in the atmosphere [1].

Musić *et al.* [2–4] investigated the phase composition, crystallinity, stoichiometry and ^{57}Fe nuclear magnetic properties of oxide precipitates formed from $FeSO_4$ solutions. The chemical and structural properties of the oxide precipitates were strongly dependent on the $[Fe^{2+}]/[OH^-]$ concentration ratio at the beginning of the precipitation process, on the rate of oxygenation, the precipitation time, the temperature and the kind of alkali (NH_4OH or NaOH) added.

The influence of sulphate anions on the formation of iron(III) oxide was investigated by the titration of acidified 6.25×10^{-2} M $Fe_2(SO_4)_3$ solution with NaOH [5]. Phase analysis of the precipitates showed the presence of the α-FeOOH, α-Fe_2O_3 and amorphous phase. It was concluded that sulphate anions could promote or suppress the formation of iron oxides, depending on the experimental conditions. The precipitation of jarosite-type compounds was not observed.

Matijević *et al.* [6] found conditions for the precipitation of monodispersed basic iron(III) sulphate particles from acidic solutions, and also emphasized the role of $FeSO_4^+$ complex in the formation of basic iron(III) sulphates [7]. Musić *et al.* [8] investigated the mechanism of the formation of iron(III) oxyhydroxides and oxides using hydrolysis of iron(III)-salt solutions at elevated temperature. The hydrolysis of Fe^{3+} ions in the nitrate and chloride solutions started with the formation of simple hydroxy complexes, and this process was followed by the formation of polymeric species. The hydroxy polymers in the nitrate solution were not presumed to include the nitrate ions in the polymer chain, whereas the polymers formed in chloride solution contained some chloride ions in place of the OH^- ions. The next step in the precipitation process was the formation of oxo-bridges and the development of α-FeOOH or β-FeOOH structure. In the sulphate solution, the formation of $FeSO_4^+$ complex suppressed the polymerization process and the formation of the oxyhydroxides and oxides. Basic iron(III) sulphates were formed instead.

The crystalline jarosite and a compound described as amorphous Fe(III) hydroxysulphate were found in the precipitates formed by the oxidation of 0.1–0.2 M $FeSO_4$ solutions with *Thiobacillus ferrooxidans* cells [9]. Bigham *et al.* [10] investigated a poorly crystallized Fe(III) oxyhydroxysulphate produced by the bacterial oxidation of Fe^{2+} in acid mine waters. The

0022–2461

content of the crystal unit-cell of this compound was determined as $Fe_{16}O_{16}(OH)_{12}(SO_4)_2$. The stoichiometry of this compound varied up to $Fe_{16}O_{16}(OH)_{10}(SO_4)_3$.

The precipitation of jarosite-type compounds was extensively investigated by Dutrizac *et al.* [11–18], because this precipitation process is important in metallurgy. For instance, in the zinc industry, the precipitation of jarosites can be used to remove excess of iron, sulphate and alkali ions from zinc sulphate–sulphuric acid solutions. The advantages of this process include the excellent settling and filtration properties of the precipitates, and low losses of divalent metals, such as Zn^{2+}, Cu^{2+} and Ni^{2+}.

Iron jarosites are described by the general formula $MFe_3(OH)_6(SO_4)_2$, $M = H_3O^+, Na^+, K^+, Rb^+, Ag^+, Tl^+, NH_4^+, \frac{1}{2}Pb^{2+}$ or $\frac{1}{2}Hg^{2+}$. They can be used as raw material for the production of iron oxide pigments. The experimental conditions for the conversion of jarosite-type compounds into iron oxides were investigated [19, 20]. Musić *et al.* [21] also investigated the thermal decomposition of basic iron(III) sulphates.

The aim of the present investigation was to obtain more information about chemical and structural properties of the precipitates generated by the hydrolysis of Fe^{3+} ions in $Fe_2(SO_4)_3$ solutions. It is known that small changes of the experimental conditions can affect significantly the phase composition and morphology of particles formed by hydrolysis of Fe^{3+} ions. For this reason, in the present work the number of experimental parameters, which affected the process of hydrolysis of Fe^{3+} ions, was restricted. $Fe_2(SO_4)_3$ solutions were heated at elevated temperature in order to accelerate the hydrolysis of Fe^{3+} ions. Three parameters were controlled during the precipitation process: (a) initial concentration of $Fe_2(SO_4)_3$ solution, (b) temperature, and (c) precipitation time.

2. Experimental procedure

The precipitations were performed in glass autoclaves (Schott, Germany) at 90 or 120 °C. Precipitates were washed with bidistilled water. The separation of the precipitate from the mother liquor was performed using a Sorvall RC2-B ultra-speed centrifuge (maximum 20000 r.p.m.). Experimental conditions for the precipitation of hydrolytical products from $Fe_2(SO_4)_3$ solutions are given in Tables I and II.

Structural properties of precipitates were investigated by X-ray diffraction (XRD), ^{57}Fe Mössbauer spectroscopy and Fourier transform–infrared spectroscopy (FT–IR), while the shape of particles was investigated by transmission electron microscopy (TEM). X-ray diffraction (XRD) powder patterns were taken at room temperature using a counter diffractometer with monochromatized CuK_α radiation (Philips diffractometer, proportional counter and graphite monochromator). XRD patterns were interpreted using data available in the literature [22]. ^{57}Fe Mössbauer spectra were recorded using equipment made by Wissel. Mössbauer spectra were fitted using the SIRIUS program. All FT–IR spectra were recorded with spectrometer made by Perkin–Elmer. The specimens were pressed into disc form using spectroscopically pure KBr. In the present paper the FT–IR spectra are presented as relative transmittance versus the wave number. Transmission electron microscopy was performed with an electron microscope made by Opton.

TABLE I Experimental conditions for the precipitation of the hydrolytical products in $Fe_2(SO_4)_3$ solutions (samples S_1–S_{11})

Samples	Concentration of $Fe_2(SO_4)_3$ solution (M)	Heating temperature (°C)	Heating time (h)
S_1	0.005	90	6
S_2	0.005	90	24
S_3	0.005	90	72
S_4	0.03	90	6
S_5	0.03	90	24
S_6	0.03	90	48
S_7	0.03	90	72
S_8	0.1	90	6
S_9	0.1	90	24
S_{10}	0.1	90	48
S_{11}	0.1	90	72

TABLE II Experimental conditions for the precipitation of the hydrolytical products in $Fe_2(SO_4)_3$ solutions (samples S_{12}–S_{21})

Samples	Concentration of $Fe_2(SO_4)_3$ solution (M)	Heating temperature (°C)	Heating time (h)
S_{12}	0.03	120	6
S_{13}	0.03	120	24
S_{14}	0.03	120	72
S_{15}	0.1	120	6
S_{16}	0.1	120	24
S_{17}	0.1	120	72
S_{18}	0.5	120	6
S_{19}	0.5	120	24
S_{20}	0.5	120	48
S_{21}	0.5	120	72

3. Results and discussion

The results of XRD phase analysis of all samples are given in Tables III and IV. XRD powder patterns of samples S_1, S_2 and S_3, shown in Fig. 1, can be ascribed to α-FeOOH, goethite. XRD lines are broadened and this effect can be interpreted in terms of poor crystallinity of precipitated goethite and small size of crystallites. Fig. 2 shows XRD powder pattern of sample S_9 with well-defined diffraction lines, which correspond to $H_3OFe_3(OH)_6(SO_4)_2$, hydronium jarosite. The phase analysis of precipitates indicated that at lower $Fe_2(SO_4)_3$ concentrations goethite was formed as a single phase, while at higher $Fe_2(SO_4)_3$ concentrations hydronium jarosite was formed alone. These results can be explained by a high tendency of Fe^{3+} ions at lower concentrations to make hydroxy complexes which undergo polymerization. On the other hand, at higher concentrations of Fe^{3+} the formation of the

TABLE III X-ray diffraction phase analysis of the precipitates formed from $Fe_2(SO_4)_3$ solutions (samples S_1–S_{11})

Sample	Phase composition
S_1	α-FeOOH
S_2	α-FeOOH
S_3	α-FeOOH
S_4	α-FeOOH, $H_3OFe_3(OH)_6(SO_4)_2$
S_5	α-FeOOH
S_6	α-FeOOH
S_7	α-FeOOH
S_8	System not analysed
S_9	$H_3OFe_3(OH)_6(SO_4)_2$
S_{10}	$H_3OFe_3(OH)_6(SO_4)_2$
S_{11}	$H_3OFe_3(OH)_6(SO_4)_2$

TABLE IV X-ray diffraction phase analysis of the precipitates formed from $Fe_2(SO_4)_3$ solutions (samples S_{12}–S_{21})

Sample	Phase composition
S_{12}	α-FeOOH
S_{13}	α-FeOOH
S_{14}	α-FeOOH
S_{15}	$H_3OFe_3(OH)_6(SO_4)_2$, $2Fe_2O_3{\cdot}SO_3{\cdot}5H_2O$
S_{16}	$H_3OFe_3(OH)_6(SO_4)_2$, $2Fe_2O_3{\cdot}SO_3{\cdot}5H_2O$
S_{17}	$H_3OFe_3(OH)_6(SO_4)_2$, $2Fe_2O_3{\cdot}SO_3{\cdot}5H_2O$
S_{18}	System not analysed
S_{19}	System not analysed
S_{20}	$H_3OFe_3(OH)_6(SO_4)_2$
S_{21}	$H_3OFe_3(OH)_6(SO_4)_2$

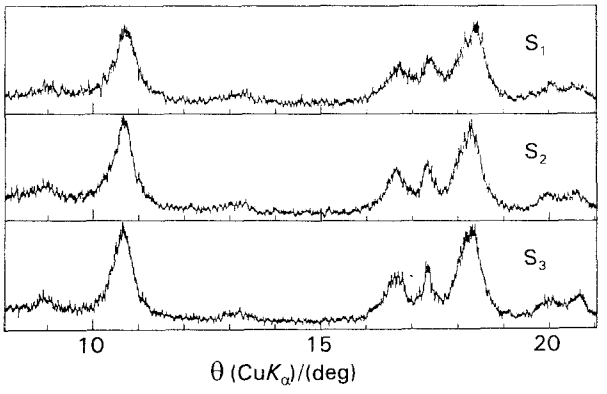

Figure 1 Characteristic parts of XRD powder patterns of samples S_1, S_2 and S_3, showing α-FeOOH.

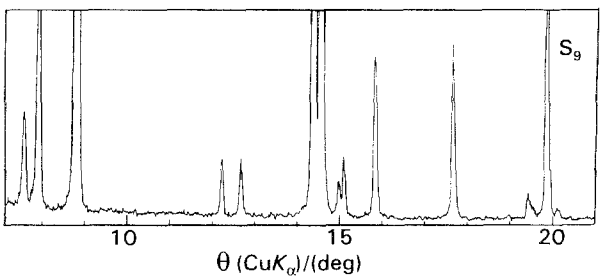

Figure 2 Characteristic parts of X-ray diffraction powder pattern of sample S_9, showing $H_3OFe_3(OH)_6(SO_4)_2$.

$FeSO_4^+$ complex strongly suppresses the polymerization of hydroxy complexes and precipitation of goethite. Similar effects were observed for other Fe(III)-salt solutions. For instance, in stock solution, 2–4 M $FeCl_3$, the chloride complexes of Fe^{3+} are dominant and there is strong suppression of the hydrolysis. However, in diluted $FeCl_3$ solutions there is a relatively fast hydrolysis of Fe^{3+}, even at room temperature, and the precipitation of β-FeOOH occurs.

Fig. 3 shows XRD powder patterns of samples S_{14}, S_{17} and S_{21}. These samples were prepared at 120 °C. XRD patterns of samples S_{14} and S_{21} corresponded to goethite and hydronium jarosite, respectively. The XRD pattern of sample S_{17} showed diffraction lines of

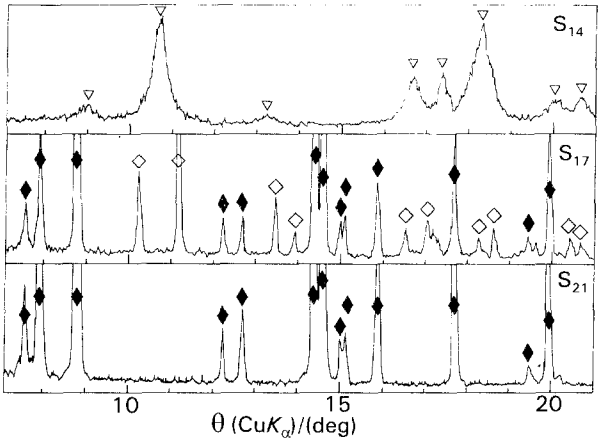

Figure 3 Characteristic parts of X-ray diffraction powder patterns of samples S_{14}, S_{17} and S_{21}: (▽) α-FeOOH, (◆) $H_3OFe_3(OH)_6(SO_4)_2$, (◇) $2Fe_2O_3{\cdot}SO_3{\cdot}5H_2O$.

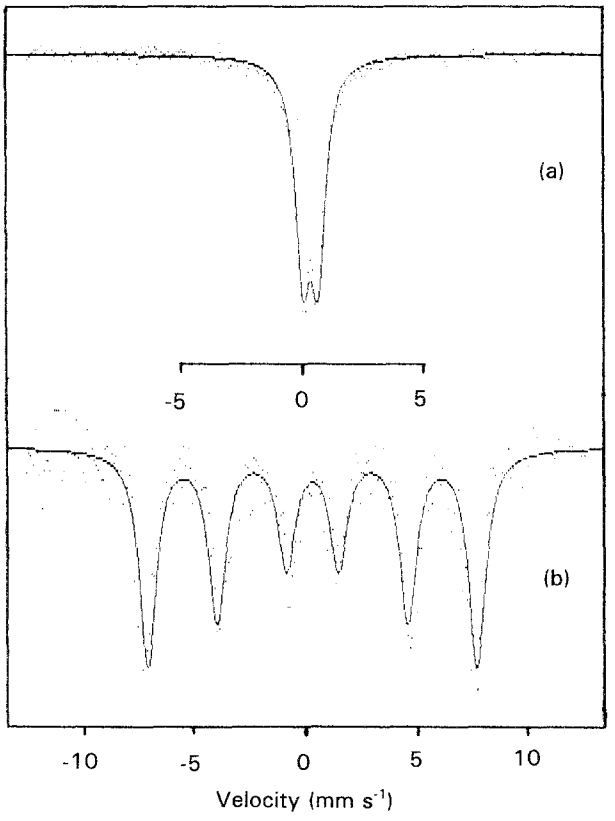

Figure 4 ^{57}Fe Mössbauer spectra of sample S_1, recorded at (a) RT and (b) 80 K.

hydronium jarosite, while the additional lines were ascribed to $2Fe_2O_3 \cdot SO_3 \cdot 5H_2O$.

Mössbauer spectra of the samples containing goethite showed a quadrupole doublet at RT and hyperfine magnetic splitting at 80 K, thus indicating the superparamagnetic character of precipitated goethite. Spectra of superparamagnetic goethite, sample S_1, recorded at RT and 80 K, are shown in Fig. 4. Fig. 5

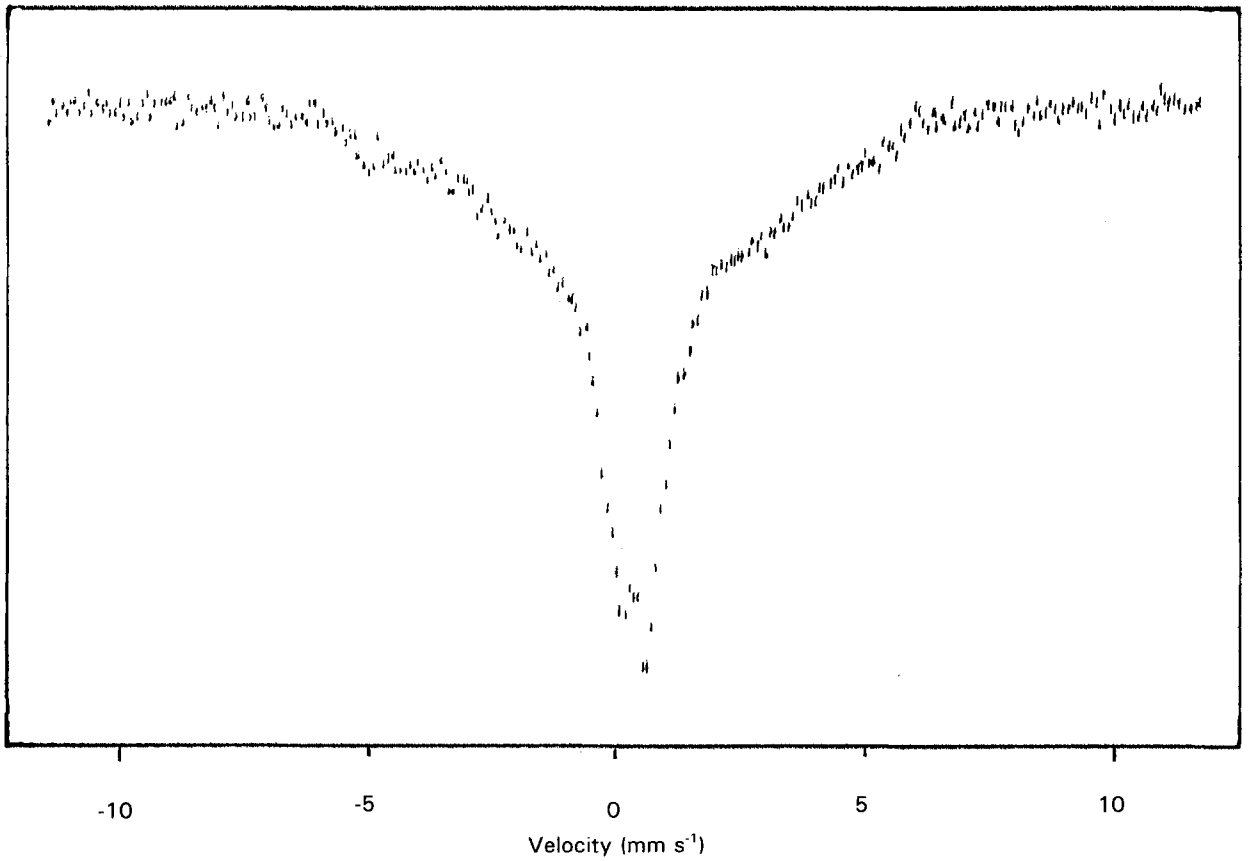

Figure 5 ^{57}Fe Mössbauer spectrum of sample S_3, recorded at RT.

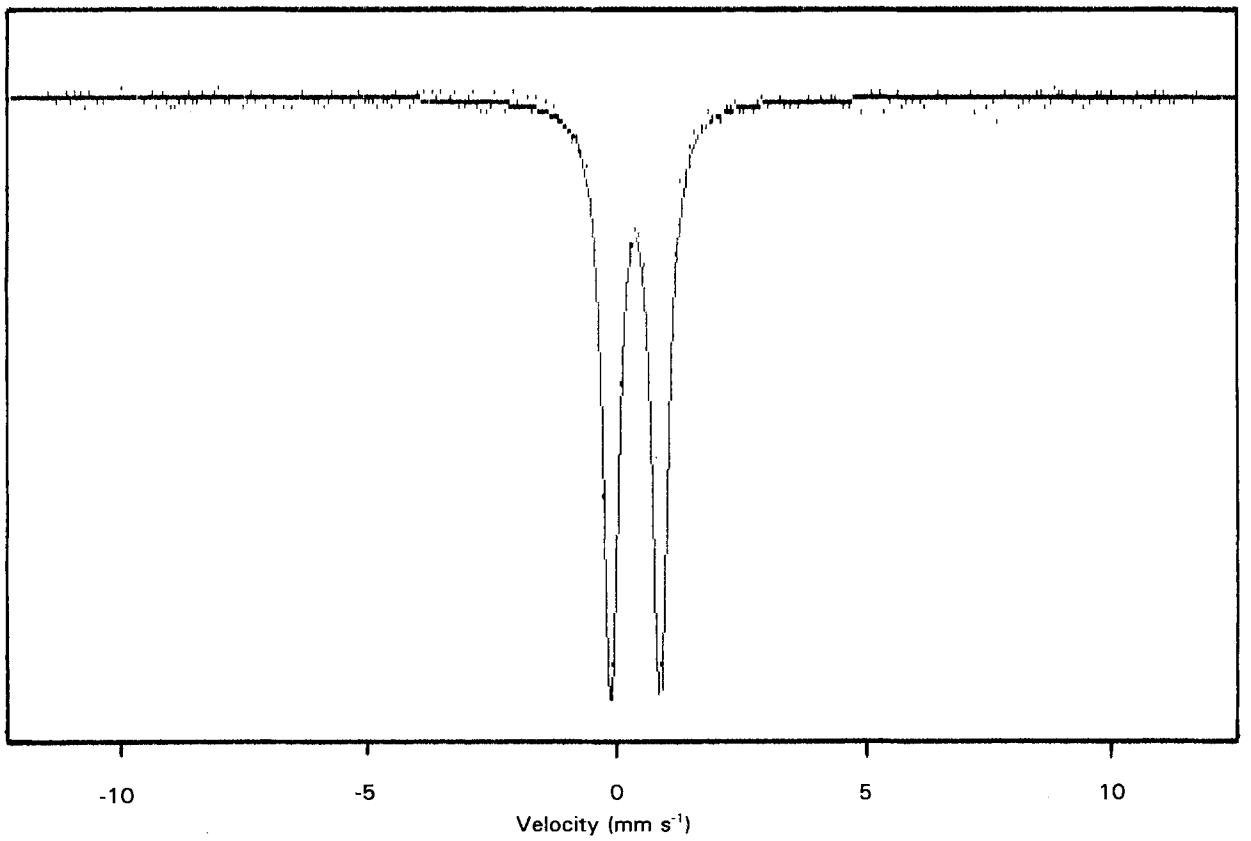

Figure 6 ^{57}Fe Mössbauer spectrum of sample S_{10}, recorded at RT.

TABLE V ^{57}Fe Mössbauer parameters calculated for the selected samples

Sample	Temperature	Isomer shift, δ^* ($mm\,s^{-1}$)[a]	Quadrupole splitting, Δ ($mm\,s^{-1}$)	HMF (kOe)	Line width, Γ ($mm\,s^{-1}$)	Identification
S_1	RT	0.357	0.627		0.747	α-FeOOH
	80 K	0.436	− 0.255	460	0.830	
S_9	RT	0.378	0.995		0.356	$H_3OFe_3(OH)_6(SO_4)_2$
S_{10}	RT	0.362	0.997		0.372	$H_3OFe_3(OH)_6(SO_4)_2$
S_{15}	RT	0.378	1.133		0.358	$H_3OFe_3(OH)_6(SO_4)_2$
		0.379	0.868		0.395	$Fe_4(OH)_{10}SO_4$
S_{16}	RT	0.380	1.008		0.390	$H_3OFe_3(OH)_6(SO_4)_2$
		0.368	0.590		0.405	$Fe_4(OH)_{10}SO_4$
S_{17}	RT	0.381	0.982		0.377	$H_3OFe_3(OH)_6(SO_4)_2$
		0.364	0.525		0.395	$Fe_4(OH)_{10}SO_4$

[a] δ^* isomer shift is given relative to α-Fe.

shows Mössbauer spectrum of samples S_3 recorded at room temperature. This spectrum shows the central quadrupole doublet and the collapsing sextet. At 80 K, the Mössbauer spectrum of sample S_3 also showed the hyperfine magnetic splitting (sextet). The Mössbauer spectrum of hydronium jarosite, precipitated from $Fe_2(SO_4)_3$ solution at 90 °C, sample S_{10}, is shown in Fig. 6. Mössbauer parameters (Table V) calculated for hydronium jarosite, which was precipitated as a single phase, are in accordance with the literature data. Leclerc [23] published the following Mössbauer parameters (RT) for the compound $H_3OFe_3(OH)_6(SO_4)_2$: $\delta_{Fe} = 0.38$–$0.39\ mm\,s^{-1}$ and $\Delta = 1.00$–$1.10\ mm\,s^{-1}$.

Fig. 7 shows Mössbauer spectra of samples S_{15}, S_{16} and S_{17}, recorded at room temperature. These spectra were evaluated as the superposition of two doublets. It is shown in Table V that the quadrupole splitting of the first doublet, Δ_1, decreased from 1.133 for sample S_{15} to $0.982\ mm\,s^{-1}$ for sample S_{17}. Quadrupole splitting of the second doublet, Δ_2, changed from $0.868\ mm\,s^{-1}$ for sample S_{15} to $0.525\ mm\,s^{-1}$ for sample S_{17}. Gancedo and Martinez [24] published the following Mössbauer parameters (RT) for $Fe_4(OH)_{10}SO_4$ ($2Fe_2O_3{\cdot}SO_3{\cdot}5H_2O$), which was obtained as the corrosion product: $\delta_{Fe} = 0.35 \pm 0.03\ mm\,s^{-1}$ and $\Delta = 0.55 \pm 0.03\ mm\,s^{-1}$. The observed decrease of Δ_2 values is probably influenced by the changes in the stoichiometry of the corresponding iron(III) basic sulphate.

Transmission electron microscopy (TEM) of goethite precipitates showed that small α-FeOOH particles were aggregated in near spherical agglomerates, as illustrated in Fig. 8. α-FeOOH agglomerates could be dispersed using an ultrasonic bath. Particles of hydronium jarosite were much bigger than those of goethite, showing an irregular shape. On the basis of TEM pictures, a clear distinction between α-FeOOH and $H_3OFe_3(OH)_6(SO_4)_2$ particles could be made, which was not possible between particles of $H_3OFe_3(OH)_6(SO_4)_2$ and $Fe_4(OH)_{10}SO_4$ (Fig. 9).

Fig. 10 shows FT–IR spectra of samples S_1 and S_3 containing goethite. These spectra are of the same type, and for this reason, only the bands characteristic for sample S_1 will be interpreted. A very strong and broad band at $3187\ cm^{-1}$ with a shoulder at $3384\ cm^{-1}$ were observed. The band at $3187\ cm^{-1}$ is

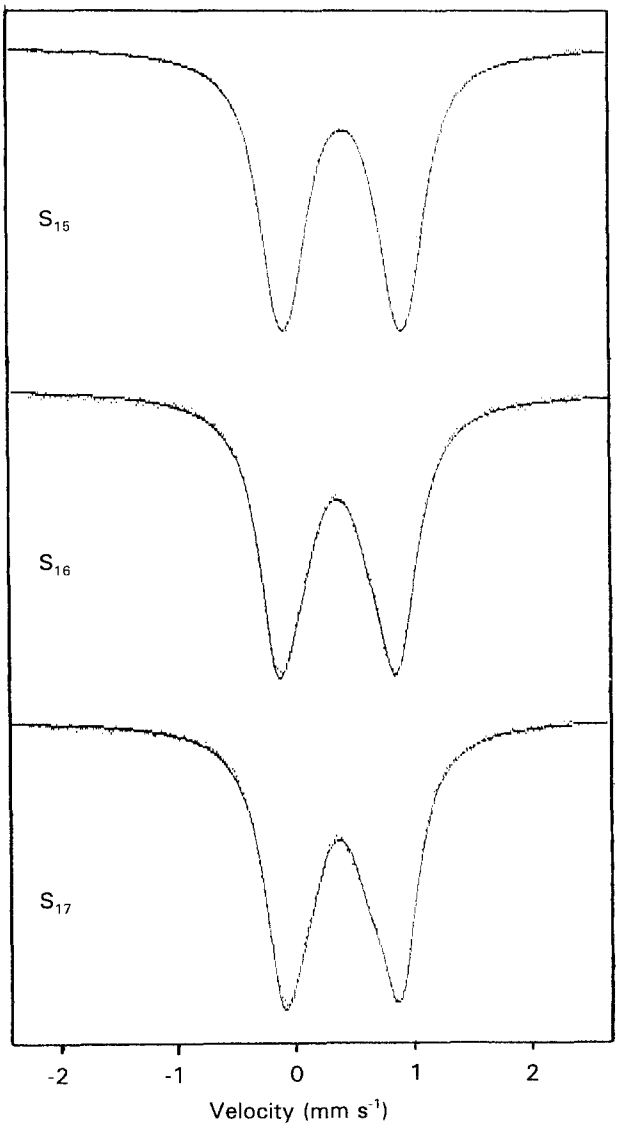

Figure 7 ^{57}Fe Mössbauer spectra of samples S_{15}, S_{16} and S_{17}, recorded at RT.

due to the presence of the OH stretching mode in goethite. The shoulder at $3384\ cm^{-1}$ can be ascribed to stretching modes of surface water molecules or to the envelope of hydrogen-bonded surface OH groups [25]. The band at $1636\ cm^{-1}$ is usually interpreted as the H_2O bending mode. Two characteristic bands at

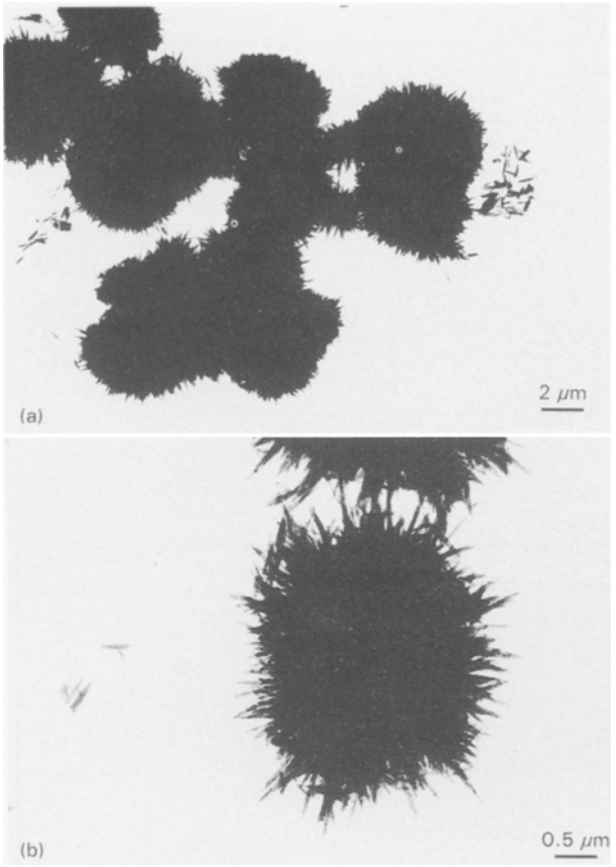

Figure 8 Transmission electron micrograph of samples (a) S_{14} and (b) S_{13}.

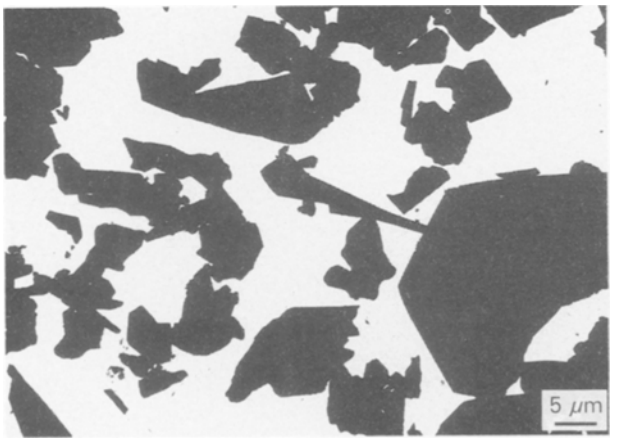

Figure 9 Transmission electron micrograph of sample S_{16}.

887 and 794 cm^{-1} can be assigned to Fe–O–H bending vibrations in goethite. Verdonck *et al.* [26] applied a method of normal coordinate analysis (NCA) in the interpretation of the IR spectrum of α-FeOOH. Observed and calculated vibrational frequencies for α-FeOOH and deuterated α-FeOOD were compared. The observed bands at 630, 495 and 270 cm^{-1} were rather insensitive to deuteration, and on the basis of this fact, they were ascribed to Fe–O stretching vibrations [26]. Cambier [27] observed a band at 3150 cm^{-1}, due to the OH stretching mode, and two bands at 892 and 795 cm^{-1}, due to the OH

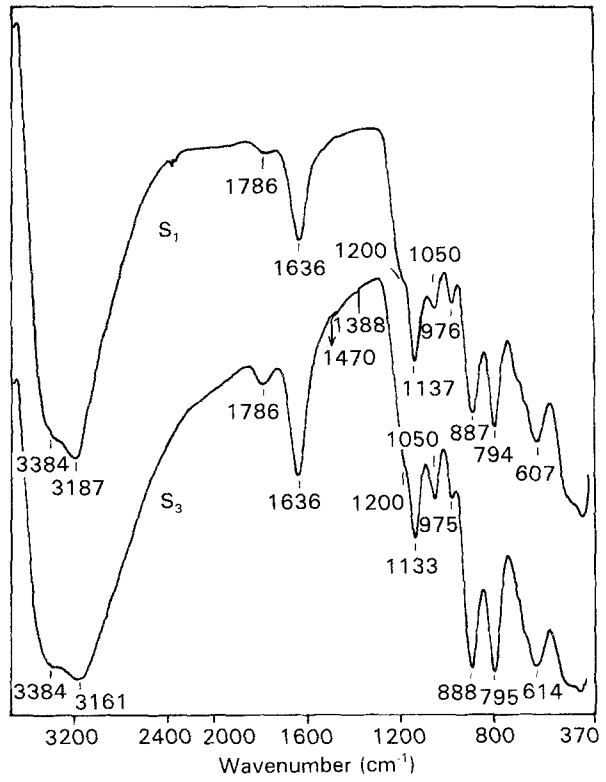

Figure 10 FT–IR spectra of samples S_1 and S_3, recorded at RT.

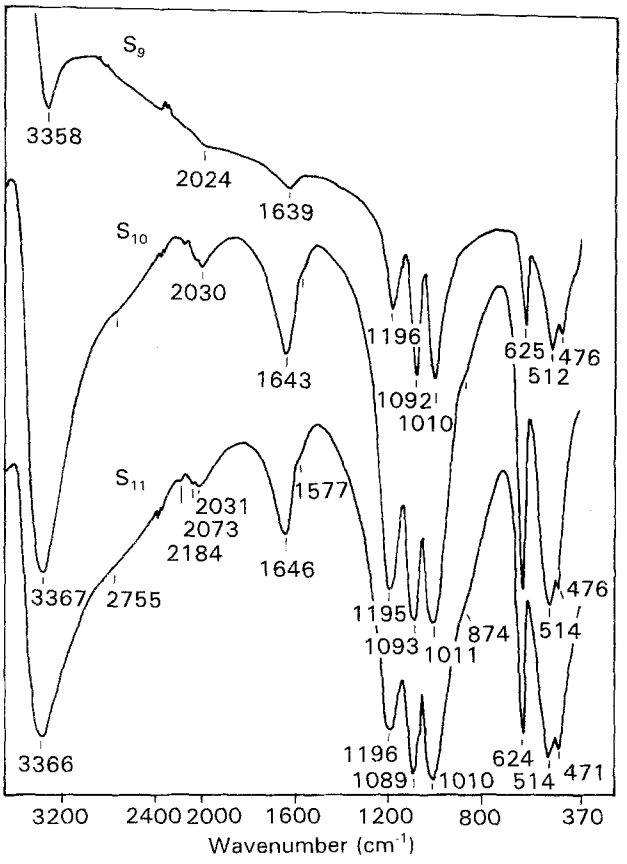

Figure 11 FT–IR spectra of samples S_9, S_{10} and S_{11}, recorded at RT.

bending modes, in goethite. The interpretation of bands below 650 cm^{-1} was similar to that of Verdonck *et al.* [26]. It was also observed that the intense IR band around 630 cm^{-1} was affected by the shape of the goethite particles.

The FT–IR spectrum of sample S_1 also showed bands at 976, 1050 and 1137 cm^{-1} with the shoulder at 1200 cm^{-1}. The band at 976 cm^{-1} can be interpreted as $\nu_1(SO_4)$ frequency, while the bands at 1050, 1137 cm^{-1} and the shoulder at 1200 cm^{-1} can be interpreted as $\nu_3(SO_4)$ frequencies. These vibrational frequencies can be attributed to specifically adsorbed SO_4^{2-} ions on the external, as well as on the internal surfaces of the goethite particles. Because the precipitation of goethite occurred at low pH values, the precipitates showed a high affinity for sulphate anions. It is known that specifically adsorbed anions, for instance, IO_3^-, CrO_4^{2-} or SO_4^{2-} have their absorption maxima at low pH values [28–30]. With increase of pH, the specific adsorption of these anions on the oxide surface decreases; this behaviour being opposite in relation to the specific adsorption of metal cations.

Fig. 11 shows FT–IR spectra of samples S_9, S_{10} and S_{11} containing $H_3OFe_3(OH)_6(SO_4)_2$. These spectra are of the same type and for this reason, their vibrational frequencies will be interpreted using the spectrum of sample S_{11}. The FT–IR spectrum of sample S_{11} is characterized with a very strong and broad band at 3366 cm^{-1} corresponding to the ν(OH) stretching frequencies, while the characteristic band at 1646 cm^{-1} is due to the H_2O bending mode. Strong bands at 1196, 1089 and 1010 cm^{-1} were also recorded for sample S_{11}. In accordance with Serna *et al.* [31] the bands at 1196 and 1089 cm^{-1} correspond to the $\nu_3(SO_4)$ frequency, while the band at 1010 cm^{-1} can be ascribed to the $\nu_1(SO_4)$ frequency. The strong and sharp band at 624 cm^{-1} can be ascribed to the $\nu_4(SO_4)$ frequency of lattice sulphates. The Fe–O lattice vibrations are characterized by the bands at 504 and 471 cm^{-1}.

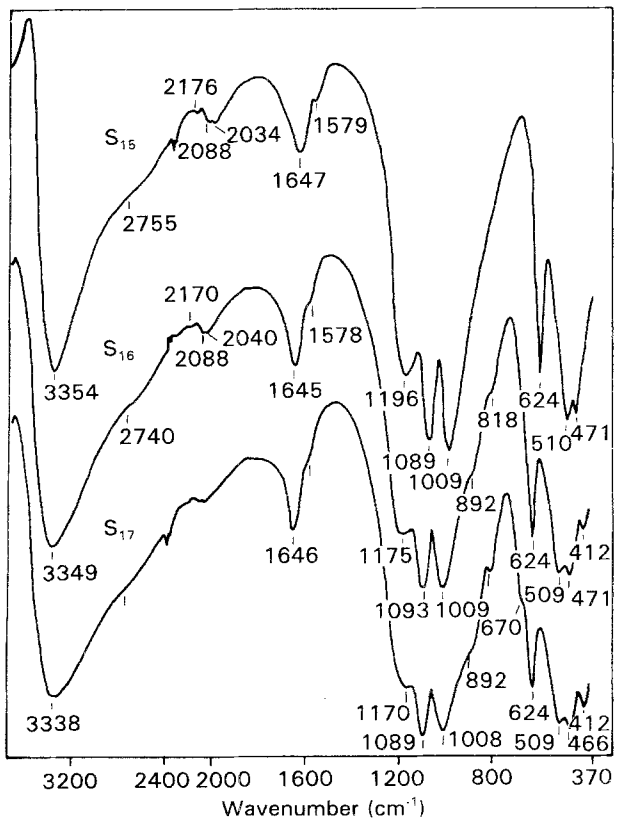

Figure 12 FT–IR spectra of samples S_{15}, S_{16} and S_{17}, recorded at RT.

Botto *et al.* [32] investigated some crystalline sulphates of the type $M_3In(SO_4)_3$, $M = K^+$, Rb^+, Cs^+, Tl^+ or NH_4^+. In their IR spectra the authors observed a band at $\simeq 870$ cm^{-1} which was attributed to a water-liberational mode. This IR band showed a tendency to disappear with removal of water from hydrated $M_3In(SO_4)_3$.

Fig. 12 shows FT–IR spectra of samples S_{15}, S_{16} and S_{17} which contained $H_3OFe_3(OH)_6(SO_4)_2$ and $2Fe_2O_3SO_3H_2O$. The main difference in relation to the spectrum of pure $H_3OFe_3(OH)_6(SO_4)_2$ (Fig. 11) occurred in the region corresponding to $\nu_3(SO_4)$ and $\nu_1(SO_4)$ frequencies. The band at 1196 cm^{-1}, observed for sample S_{15}, became a shoulder at 1170 cm^{-1} for sample S_{17}. The spectrum of sample S_{17} also showed a well-pronounced shoulder at 892 cm^{-1}. The FT–IR spectra of all other samples, prepared in the present work, were in accordance with the type-spectra shown in Figs 10–12.

Acknowledgement

We thank Dr N. Ljubešić for assistance in TEM work.

References

1. H. LEIDHEISER, Jr and S. MUSIĆ, *Corros. Sci.* **22** (1982) 1089.
2. S. MUSIĆ, I. CZAKÓ-NAGY, S. POPOVIĆ, A. VÉRTES and M. TONKOVIĆ, *Croat. Chem. Acta* **59** (1986) 833.
3. S. MUSIĆ, S. POPOVIĆ and M. GOTIĆ, *ibid.* **60** (1987) 661.
4. *Idem, J. Mater. Sci.* **25** (1990) 3186.
5. J. DOUSMA, D. DEN OTTELANDER and P. L. DE BRUYN, *J. Inorg. Nucl. Chem.* **41** (1979) 1565.
6. E. MATIJEVIĆ, R. S. SAPIESZKO and J. B. MELVILLE, *J. Coll. Interface Sci.* **50** (1975) 567.
7. R. S. SAPIESZKO, R. C. PATEL and E. MATIJEVIĆ, *J. Phys. Chem.* **81** (1977) 1061.
8. S. MUSIĆ, A. VÉRTES, G. W. SIMMONS, I. CZAKÓ-NAGY and H. LEIDHEISER Jr, *J. Coll. Interface Sci.* **85** (1982) 256.
9. N. LAZAROFF, W. SIGAL and A. WASSERMANN, *Appl. Environ. Microbiol.* **43** (1982) 924.
10. J. M. BIGHAM, U. SCHWERTMANN, L. CARLSON and E. MURAD, *Geochim. Cosmochim. Acta* **54** (1990) 2743.
11. J. E. DUTRIZAC and S. KAIMAN, *Hydrometall.* **1** (1975) 51.
12. J. E. DUTRIZAC and T. T. CHEN, *Canad. Mineral.* **19** (1981) 559.
13. J. E. DUTRIZAC, in "Proceedings of the Australian Institute of Mining and Metallurgy, No. 278 (Australian Institute of Mining and Metallurgy, Parkville, Victoria 3052, Australia, 1981) pp. 23–32.
14. J. E. DUTRIZAC, *Metall. Trans. B* **14** (1983) 531.
15. J. E. DUTRIZAC, in "Hydrometallurgical Process Fundamentals", edited by R. G. Bautista (Plenum, 1984) pp. 125–69.
16. J. A. RIPMEESTER, C. I. RATCLIFFE, J. E. DUTRIZAC and J. L. JAMBOR, *Canad. Mineral.* **24** (1986) 435.
17. J. E. DUTRIZAC and J. L. JAMBOR, in "Applied Mineralogy", edited by W. C. Park, D. M. Hausen and R. D. Hagni (Metallurgical Society American Institute of Mining, Metallurgy and Petroleum Engineering, Warrendale, PA, 1985) pp. 507–30.
18. *Idem, Hydrometall.* **17** (1987) 251.
19. W. KUNDA and H. VELTMAN, *Metall. Trans B.* **10** (1979) 439.
20. J. E. DUTRIZAC, in "Productivity and Technology in the Metallurgical Industries", edited by M. Koch and J. C. Taylor (Minerals, Metals and Materials Society, 1989) pp. 587–612.

21. S. MUSIĆ, A. VÉRTES, G. W. SIMMONS, I. CZAKÓ-NAGY and H. LEIDHEISER Jr, *Radiochem. Radioanal. Lett.* **49** (1981) 315.
22. International Centre for Diffraction Data, Joint Committee on Powder Diffraction Standards, Powder Diffraction File, 1601 Park Lane, Swarthmore, PA 19081, USA.
23. A. LECLERC, *Phys. Chem. Mineral.* **6** (1980) 327.
24. J. R. GANCEDO and M. L. MARTINEZ, in "Magnetic Resonance in Colloid and Interface Science", edited by J. P. Fraissard and H. A. Resing (Reidel, 1980) p. 371.
25. C. MORTERRA, A. CHIORINO and E. BORELLO, *Mater. Chem. Phys.* **10** (1984) 119.
26. L. VERDONCK, S. HOSTE, F. F. ROELANDT and G. P. VAN DER KELEN, *J. Molec. Struct.* **79** (1982) 273.
27. P. CAMBIER, *Clay Minerals* **21** (1986) 191.
28. S. MUSIĆ, J. ŠIPALO-ŽULJEVIĆ and R. H. H. WOLF, *Radiochim. Radioanal. Lett.* **45** (1980) 235.
29. S. MUSIĆ, J. ŠIPALO-ŽULJEVIĆ, *Radiochim. Acta* **27** (1980) 61.
30. S. MUSIĆ, M. RISTIĆ and M. TONKOVIĆ, *Z. Waser-Abwaser Forsch.* **19** (1986) 186.
31. C. J. SERNA, C. PARADA CORTINA and J. V. GARCIA-RAMOS, *Spectrochim. Acta* **42A** (1986) 729.
32. I. L. BOTTO, E. J. BARAN and A. C. GARCIA, *An. Quim.* **83B** (1987) 145.

Received 1 October 1992
and accepted 19 October 1993